Applied Materials Today 27 (2022) 101471

Contents lists available at ScienceDirect

Applied Materials Today

journal homepage: www.elsevier.com/locate/apmt

Unraveling the distinct germination processes of sporopollenin-based pollen grains and spores through morphological analyses upon natural nano-architectonics process

Qian Shi[a], Mohammed Shahrudin Bin Ibrahim[b], Xingyu Zhang[c], Youngkyu Hwang[b], Hokyun Chin[b], Shengyang Chen[a], Wen See Tan[a], Hua Li[c], Juha Song[a,*], Nam-Joon Cho[b,*]

[a] School of Chemical and Biomedical Engineering, Nanyang Technological University, 62 Nanyang Drive, Singapore 637459, Singapore
[b] School of Materials Science and Engineering, Nanyang Technological University, 50 Nanyang Avenue, Singapore 639798, Singapore
[c] School of Mechanical and Aerospace Engineering, Nanyang Technological University, 50 Nanyang Avenue, Singapore 639798, Singapore

ARTICLE INFO

Article history:
Received 8 February 2022
Revised 1 April 2022
Accepted 2 April 2022

Keywords:
Pollen
Bioinspired materials
Germination
Spore
Biomechanics

ABSTRACT

The outermost exine capsules of many pollen and spore grains are composed of a chemically inert yet mechanically robust sporopollenin biopolymer. These dynamically expansible and foldable capsules have great potential as renewable functional biomaterials with industrial applications. However, the mechanical and morphological variations in the shape, size, robustness, and apertural strength of the exine capsules across taxa of angiosperms and cryptogamic plants remains poorly understood. Thus, in this study, we unraveled the abortive microgel transformation of spores inspired by their germination mechanism, being compared with eudicot-based pollen microgels. After chemical treatments, significant mechanical degradation of exine was clearly observed for the *Camellia* pollen, whereas crosslinking density and modulus of spore exine remained almost constant. The significant volume expansion of *Camellia* pollen was observed akin to sunflower pollen; in contrast, the spores ballooned showed limited volume changes under equal levels of turgor pressure. Furthermore, spore underwent marked changes in volume when their aperture sutures were softened and ruptured, which are prerequisites for spore germination. Therefore, this study disentangled mechanical and morphological origins of biochemical pathways of pollen and spore germination, and germination-like hydration and desiccation, which will give clues about selection of pollen and spore species for potential biomaterial applications.

1. Introduction

Pollen and spore grains are some of the most durable natural materials on earth. Their largely indestructible bi-layered shells consist of an outer layer (exine) of sporopollenin-based and an inner layer (intine) of cellulose and pectin [1]. During harmomegathy, the pollen shell protects the enclosed gametophytic nucleus from mechanical impact, dehydration, and biological and chemical toxins [2–6]. However, the sporopollenin-rich exine must be sufficiently elastic to support the deformation of pollen and spores during germination [7–9], as the germination process is initiated by biochemical mechanisms that soften the tough sporopollenin-dominant exine and convert the intine into a swellable hydrogel. During germination [10–12], the intine [13,14] – which is cross-linked with cellulose microfibril and hemicellulose [15] – plays a crucial role in expanding the pollen shell: intine acts as an osmotic stress motor, driving the overlying softened exine to close off or open up its apertures [7,13,14,16-19].

Inspired by pollen germination, a facile strategy that mimics traditional soapmaking was devised to transform hard pollen grains into soft, stimuli-responsive microgel particles (Fig. 1). This strategy worked well with certain pollen species, such as eudicots. However, it did not work with flowering monocots, gymnosperms, or spore-bearing lycophytes, revealing the complexity of the chemical processes underlying germination in pollen grains and spores [15]. Variations in the processibility of the pollen grains from different plant species may be related to structural variations in their shell architectures, such as variations in sculpture, apertures, size, and symmetry and the range of ornamental wrinkles and spikes. For example, as specific pollen–stigma recognition [16,20] is required for effective pollination and sexual reproduction [21] in angiosperms, most eudicot pollen grains (e.g., those of *Baccharis, Helianthus* (sunflower), *Camellia, Leonurus*, and *Lotus*) [15,22] have spherical or ellipsoidal shapes with three-fold symmetric tri-

* Corresponding authors.
E-mail addresses: songjuha@ntu.edu.sg (J. Song), jcho@ntu.edu.sg (N.-J. Cho).

https://doi.org/10.1016/j.apmt.2022.101471
2352-9407/

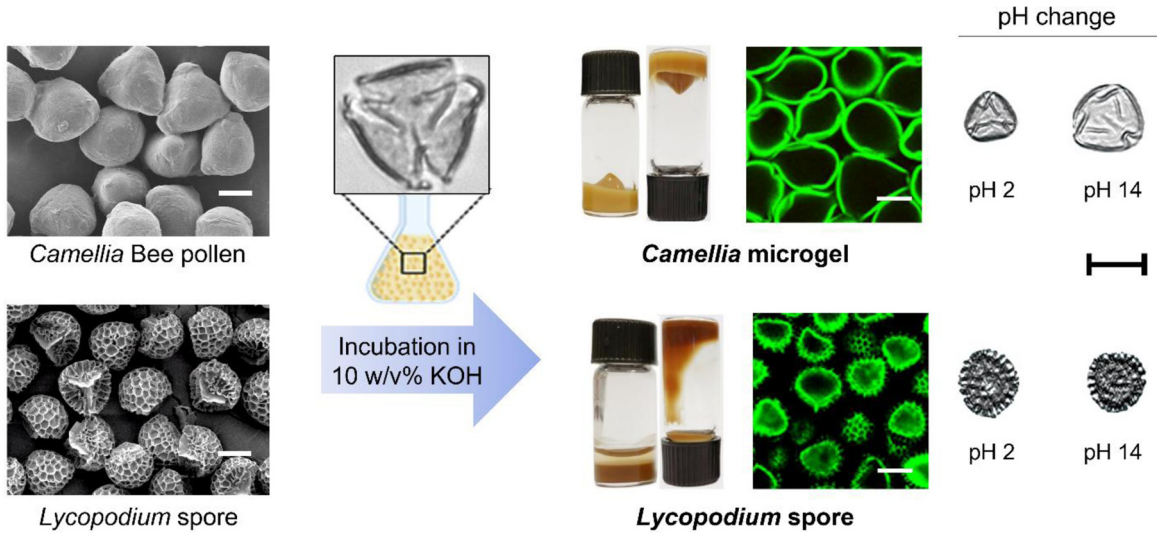

Fig. 1. Comparison of *Camellia* pollen and *Lycopodium* spores after the KOH treatment. *Camellia* pollen grains were successfully transformed into microgels, showing pH-responsive swelling behavior, whereas Lycopodium spores remained unchanged, being insensitive to pH changes. All scale bars are 20μm.

apertures [16]. In marked contrast, *Lycopodium* [23] and fern spores [24] have an asymmetric "three-fold dumpling" shape (Fig. 1). However, the deformation mechanisms of pollen and spore germination and the links between the morphological diversity and functional roles of their bi-layered microcapsules remain obscure [25,26]. Further scientific efforts are required to explore this mechanism within species and across taxa. Although the exine biopolymer protection and intine hydrogel motor features described above [13,14] are observed in both flowering plant pollens and cryptogamic spores, their germination processes are distinct.

In flowering plants, pollination is initiated when a pollen grain is loaded onto a stigma by a pollinator [27], as illustrated in Fig. 2a. Subsequently, the desiccated pollen grain gradually unfolds and expands [5,17] as it absorbs H_2O, H^+, Ca^{2+}, and other nutrients from the stigma, which further activates the germination process. This accelerates the influx of water through open channels in the porous exine and the apertures [21,28,29], resulting in substantial changes in volume [7,16,18,30]. Subsequently, the continuous intine starts protruding from the opened apertures, facilitating tubular growth [16]. Fertilization is completed when the male gametophytic sperm enclosed within the elongated pollen tube reaches the ovary through the style [31]. The resultant zygote continues to develop within the ovary, eventually forming a seed [32,33]. However, high humidity sends a false signal to pollen grains, which triggers pseudo-hydration in unreleased pollen grains in the anther [28] and in preserved mature pollen grains in vitro [30]. The same scenario occurs in dead pollen [17]. In such cases, germination may be aborted through the germination-terminated and re-germination process associated with reversible harmomegathy, which is followed by a metabolically quiescent state [34,35] that preserves pollen grains for future rehydration on suitable stigmata [10,18]. This reversible germination process has been fully explained through diffusion-based, hyperelasticity-based finite element analysis (FEA) models in conjunction with multiphysics-based pH-responsive hydrogel models [36].

However, as Fig. 2b illustrates, cryptogamic spore cells undergoing meiosis secrete spores containing both male and female gametophytes. Spore grains initiate germination after exposure to a hydrated solid medium or a liquid medium in an oxygenic atmosphere. In contrast, angiosperm pollen adheres to stigmata to trigger germination and form a zygote [27]. Water intake and subsequent cell divisions lead to osmosis and generate turgor pressure on the tightly closed spore exine, inducing the bulging of the irregular-shaped spores into regular spheres until the apertural exine is irreversibly ruptured [24]. Subsequently, the growing rhizoids associated with continuous asymmetric cell divisions are released from the large open sites of the spore apertures, and then mature into roots and protonemata [37]. Notably, no ovary is involved in zygote development; instead, the sperm and egg are released separately from the antheridium and archegonium, and ultimately mate to form a zygote that directly produces leaves, without producing seeds [11].

In this study, we hypothesized that microgel formation depends on the specific material properties of pollen and spore grains, including their wall thickness, shape, porosity, and mechanical strength. We focused on characterizing the apertures within the exine, which regulate water and ion flux. We selected *Camelia* pollen and *Lycopodium* spores as representative grains that form and do not form microgel particles, respectively. *Camellia* and *Lycopodium* have been used for medicine [38] or drug carriers [39], showing great potential for various biomedical applications. Moreover, *Camellia* pollen is more suitable for observation of the morphological change on the exine layer before and after chemical treatments, compared with the sunflower pollen grains that have the spiky surface [15]. We experimentally characterized specific features of each type of grain, including their nano/microstructures and mechanical properties, before and after chemical processing. We also performed finite element method (FEM) simulations to understand microgel formation processes and elucidate structure–property relationships.

2. Material and methods

2.1. Materials

Natural *Lycopodium* (*Lycopodium clavatum*) spores (S-type) of flowering plants and *Camellia* (*Camellia sinensis* L.) bee pollen granules of flowerless, vascular plants were purchased from Yuensun Biological Technology Co., Ltd. (Xi'an, Shaanxi, China).

2.2. Preparation of the pollen and spore microgel particles

Pollen and spore microgel suspensions were prepared following the three-step process used in our previous work. [15,40] Briefly, the three steps were (1) defatting; (2) cytoplasmic removal (first

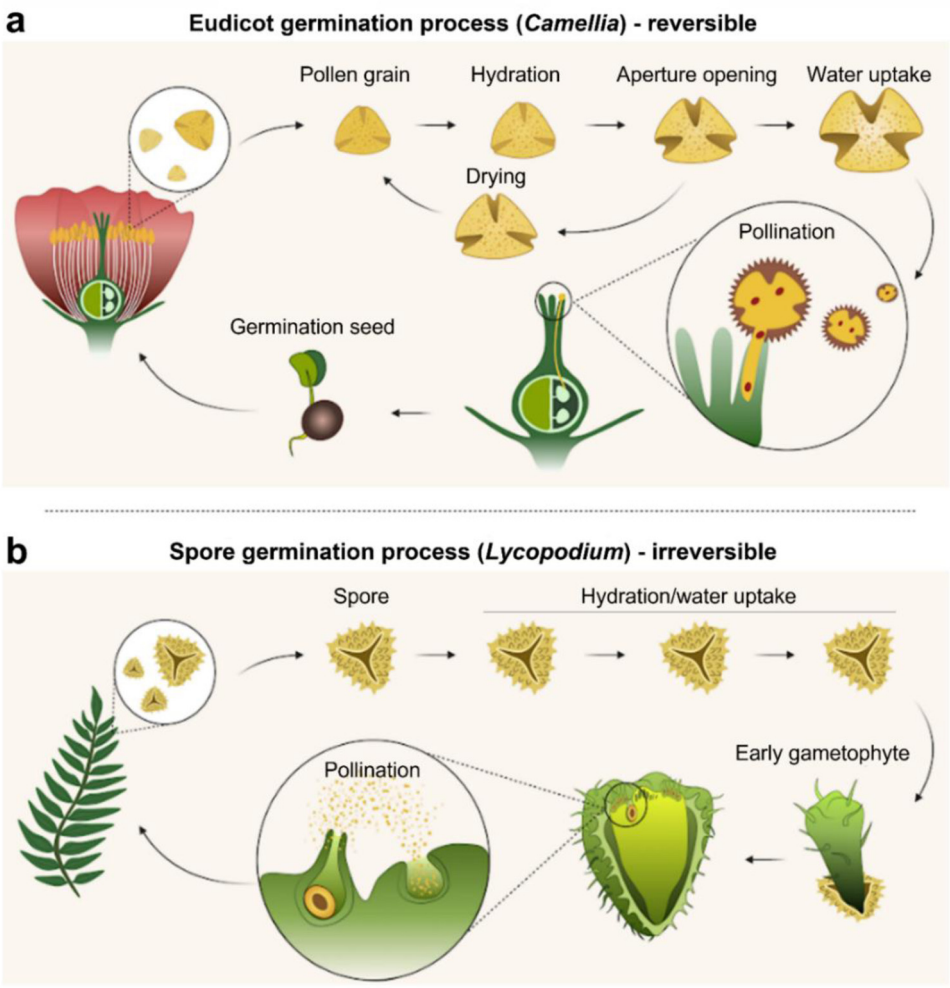

Fig. 2. Distinctive germination processes of a grain of eudicot (*Camellia*) pollen and a *Lycopodium* spore. **a,** Reversible germination of a *Camellia* pollen grain in response to drought environments. **b,** Irreversible germination of a *Lycopodium* spore in extreme environments.

KOH treatment step); and (3) microgel formation (second KOH treatment step).

2.3. Scanning electron microscopy (SEM)

To prepare defatted samples: Defatted pollen or spore particles were dried in a freeze dryer (LabConco, Kansas City, MO) under 0.008 mbar of vacuum pressure for 2 days. To prepare microgel samples: 3 μL of each sample was dispersed in 200 μL of the appropriate medium in a 1.5 mL microcentrifuge tube, and the resulting mixture was frozen with liquid nitrogen for 15 min, and then lyophilized in a freeze dryer for 2 days. The dried samples were spread and immobilized on a sample holder with copper tape, and then sputter-coated with a 10-nm thick platinum film using a JFC-1600 Auto Fine Coater (JEOL, Tokyo, Japan; operating settings, 20 mA for 40 s). For cross-sectional observation, the dried samples were adhered onto a piece of double-sided copper tape (2 cm $\times$ 1.3 cm) and dipped into liquid nitrogen for 5 min. Then, multiple cuts were conducted across the frozen sample with a surgical blade (B. Braun Melsungen AG, Melsungen, Germany). Finally, the pollen-adhered or spore-adhered copper tape was lyophilized in a freeze dryer for 2 days. Field-emission SEM imaging was performed using a JSM-7600F Schottky field-emission scanning electron microscope (JEOL) at an accelerating voltage of 5.00 kV and under various magnification levels.

2.4. Fourier-transform infrared (FTIR) spectroscopy and X-ray photoelectron spectroscopy (XPS) characterization of pollen and spores

Before the FT-IR analysis, the pollen or spore gel samples were frozen at –20 °C for 24 h, and then lyophilized in a freeze dryer (Labconco, Kansas City, MO, USA) under 0.008 mbar vacuum pressure for 2 days. The resulting dried samples were subject to FTIR spectroscopy using a PerkinElmer spectrometer (PerkinElmer, Waltham, MA, USA) equipped with a diamond cell attenuated total reflection accessory module. Reflectance infrared spectra were collected at 4000–650 cm^{-1}, with 16 scans per measurement and three replicate measurements per sample. Background spectra were collected prior to the sample readings, and automatically subtracted from each measurement. A baseline correction procedure was carried out using Spectrum 10 software (PerkinElmer). Following baseline correction, each spectrum was standardized as previously reported [41].

For XPS analysis, standard XPS methodologies were used [42]. Wide-scan (160 eV) and narrow-scan (20 eV) XPS was performed on defatted (native) and alkaline-hydrolyzed pollen grains. The samples were deposited on carbon tape (5 mm $\times$ 5 mm) adhered to a silicon wafer, and lyophilized in a freeze dryer (LabConco, Kansas City, MO) for at least 12 h prior to analyses. The samples were analyzed using an AXIS Supra (XPS) surface analy-

sis instrument (Kratos Analytical Ltd, Stretford, Greater Manchester, England) equipped with a monochromatic Al/Mg X-ray source (225 W, 2×10^{-9} mbar). The spectra were obtained using an aluminum anode (Al Kα = 1491.600 eV) and charge neutralization. The data were processed using ESCApe software (Kratos Analytical Ltd, Stretford, Greater Manchester, England).

2.5. Dynamic image particle analysis

Dynamic image particle analysis was performed using a benchtop Fluid Imaging FlowCAM system (Fluid Imaging Technologies, Scarborough, ME, USA) with a 200 μm flow cell and a 10× optical lens, as used in our previous work [15,40]. For pH-dependent studies, five different pH conditions were tested (pH 2, 4, 7, 10, and 14), which were prepared by the addition of 2 M HCl or 2 M KOH to deionized water. For each pH condition, a sample of 3 μL of pollen or spore microgel was mixed thoroughly with 700 μL of the corresponding pH solution. After an incubation period of 5 min, the pollen or spore particles were dispersed by pipetting, and then 200 μL of the suspension was passed through the flow cell.

2.6. Measurements of Young's moduli of pollen and spore

The mechanical properties of the defatted plant grains and microgel particles were characterized using atomic force microscopy (AFM) force–distance (or load versus displacement) measurements, as described in our previous work [15,40]. To analyze wet samples, defatted and alkali-treated pollen and spore samples were dispersed in an appropriate medium (50 μL), and the mixture was spread onto a petri dish (Nunc, Roskilde, Denmark) by pipette. Then, excess liquid was aspirated, and the partially hydrated samples were left on the glass slide for experimental characterization. To analyze dry specimens, pollen samples were directly spread onto the surface of a petri dish before measurement. Intact pollen or spore particles were used for extracting the Young's moduli of exines. Partially fractured particles, which exposed the intine, were used to determine the Young's modulus of intines (**Fig. S1**). To avoid the substrate effect, we followed the 10% depth rule, which specifies that the indentation depth should be less than 1/10th of the layer thickness [43]. The indentation depths for exine measurements were set in the range of 20–60 nm under indentation loads of 3–6 μN. During all of the measurements, two AFM probes were used on the NX-10 AFM instrument (Park Systems, Suwon, South Korea): (i) an Al reflex-coated silicon cantilever PPP-NCHR (Nanosensors, Neuchâtel, Switzerland) with a typical spring constant of ~42 N/m and a tip-end radius of 5 nm; and (ii) a diamond cantilever TD26135 (Micro Star Technology, Huntsville, TX) with a spring constant of ~150 N/m and a tip-end radius of 5 nm [15,40]. We confirmed that both the AFM probes provided almost identical Young's moduli for the exine and intine (**Fig. S1**). The measurements were conducted at various positions (more than 16 data points) in a 5 μm × 5 μm area at an approach speed of 0.8 μm/s with a maximum loading force of 4.8 μN and zero contact time. To remove organic contaminants, the AFM cantilever was rinsed with water and ethanol, and then treated with a UV light cleaner for 30 min prior to experiments. The spring constant and sensitivity of the deflection signal were also calibrated against the thermal vibration of the AFM cantilever using commercial software (XEP, Park Systems) [44]. The force-versus-displacement curves were corrected by subtracting the deflection distance of the AFM probe from the total displacement. In the data analysis, we used the classic Hertz model and the Johnson–Kendall–Roberts (JKR) model, and we assumed the Poisson's ratio ν for all of the samples was 0.5, which is typical for natural materials [15].

2.7. Numerical modeling for swelling/deswelling and rupturing of pollen microgel and spore particles

2.7.1. Boundary conditions for pollen and spore shells during the swelling and de-swelling process

Stress induced by proton- and/or metallic-cation complexation [45] has been observed in plant tissues, such as cell walls, pollens, pollen tubes, stalks, and woody stems, in response to biotic stimuli (e.g., salt, drought, wounds, temperature changes, and growth) and abiotic chemical treatments (e.g., pH change and Ca^{2+}/EDTA treatment) [15,46,47]. As shown in the two-dimensional schematics of a pollen grain in **Fig. S2**, typical pollen and spore shells are composed of an intine and an exine. The sporopollenin-based exine is the first line of defense, as it blocks the flow of ions or water and provides mechanical support to the shell. In contrast, after absorbing water and under ion interaction, the intine, which contains the cellulose fiber-reinforced pectin, produces and transmits a force that pushes into the exine [12]. **Fig. S2** shows a pollen grain in a stressed state due to biotic or abiotic-induced deformation. The swellable intine efficiently transfers the coupled turgor and osmosis pressures to the exine, initiating the aperture opening of the pollen and spore grains. This process subjects the exine to the radical stress σ_r and loop stress σ_θ, as it undergoes radical expansion due to increased internal pressure, which is accelerated by excessive water uptake (**Fig. S2**). Nevertheless, the layer thickness of the exine, $r_k - r_j$, and the layer thickness of the intine, $r_j - r_i$, are extremely small compared to the radius of the entire pollen shell, where r_i, r_j is the radius of the inner and outer intine surfaces. For instance, a *Camellia* pollen grain has an intine thickness of ~0.08 μm and an exine thickness of ~0.73 μm, and a shell radius of ~16 μm. Hence, the radial stress σ_r is insignificant and thus negligible for these shell-walled structures [48,49]. **Fig. S2 c-d** compare the natural pollen and spore systems during germination with artificially transformed pollen microgels during swelling [9,15]. Both illustrations show similar boundary conditions, although the factors that triggered the shell expansion were different. The key membrane tensile stress, shown as σ_θ in the schematic illustration, was induced by opening the nanoscale water/ion channels and apertures, facilitating the expansion of the living pollens during germination [5,34] and the changes in the bioinspired pollen microgels under pH or ionic treatments [15,40]. To simulate the swelling/deswelling of pollen grains and pollen microgels, we developed finite element analysis (FEA) models of the exine with the boundary conditions calculated or derived from the multiphysics models of the intine under different pH conditions. **Fig. S2 e** illustrates the exine structure in the FEA simulations of the swelling/de-swelling of *Camellia* pollen and *Lycopodium* spores. The tri-aperture on the exine was modeled with the contact cohesive interaction set for weakly or strongly bonded interfaces, which varied according to the deformation of the shells of *Camellia* pollen and *Lycopodium* spores. The expansion boundary conditions of the exine from *Camelia* pollen and *Lycopodium* spores were based on the magnitude of σ_θ or swelling pressure, $P_{i,\,swelling}$, which was determined from the multiphysics models of the intine.

2.7.2. Constitutive law for the intine based on the multiphysics model

The intine of the pollen microgel particles was assumed to be a stimuli-responsive hydrogel that provided the driving force for the inflation and deflation of the exine layer in pollen microgel particles [15]. Thus, for simplification, the equilibrium of the pollen intine swelling was modeled in the radial direction, due to its spherical symmetry. Based on our developed multiphysics models, we inputted the material parameters of *Camellia* pollen and *Lycopodium* spores to calculate the intine swelling pressure ($P_{i,\,swelling}$), minus the initial fixed-charge density in the dry state (C_m^0) (**Table S1**). C_m^0 was predicted using the multiphysics model and validated using

the FEA model for the exine. As C_m^0 is independent of the pollen intine-swelling process, the well-identified value of C_m^0 allows the modeling prediction to show good agreement with the experimental observations. The simulations were conducted using the commercial software COMSOL Multiphysics 5.3 (COMSOL Inc., Stockholm, Sweden, 1986), using partial differential equations to represent the interfaces for the ionic transport and pollen intine deformation, and the electrostatics module for the electrical distribution in the domain. We found that the average radius and Young's modulus of *Camellia* pollen were almost identical to those of *Lycopodium* spores, and both had very thin intines. Thus, the induced swelling pressure of both intine systems under changing pH conditions was similar. The swelling pressure was obtained for each pH condition, and was directly used as the inflating pressure in the exine FEA models.

2.7.3. Constitutive law for the exine

Like the exine of sunflower pollen, the exine of *Camellia* and *Lycopodium* grains was assumed be hyperelastic, allowing reversible rubber-like expansion and contraction under intine swelling pressure. Therefore, three-dimensional computational models simulating the micromechanics of the exine in pollen particles were developed, based on the classic hyperelastic neoHookean model [50]. This model requires two key material parameters: Young's modulus and a Poisson's ratio. The Young's modulus was retrieved from AFM force-based nanoindentation tests performed on the pollen particles. Given the presence of pores in the exine, a value of 0.4 for the Poisson's ratio was selected, to account for exine compressibility, as described in our previous work [15].

2.7.4. FEA modeling for the inflation/deflation of the exine of pollen and spore grains

To investigate how σ_θ or $P_{i,\ swelling}$ mediate the responses of pollen species with enormously different morphologies, we used the exine FEA models available in the commercial software package ABAQUS 2019® (Dassault Systèmes SIMULIA, Johnston, RI). The three-dimensional models for *Lycopodium* spores and *Camellia* pollen were constructed separately, as their morphologies (e.g., size and symmetry) are markedly different to the previously built sunflower exine FEA model (**Fig. S3 a)** [15,34,51]. Here, we selected the 6-h KOH-treated pollen and spore grains, and the Young's moduli were 550 MPa and 600 MPa, respectively, for *Camellia* and *Lycopodium*. These simulation results were directly compared with the expansion ratio in the experimental results (**Fig. S3 a)**. The measured radius of *Camellia* pollen was significantly changed by the pH and ionic conditions, whereas the *Lycopodium* spore did not exhibit any changes in size. The expansion ratio was defined as the ratio of the projected swollen radius (R_{swell}) of the pollen or spore to its original radius (R_0). The Camellia *pollen* and Lycopodium *spores* both had three-fold symmetry; therefore were modeled one-third of the entire pollen structure, including one aperture. Symmetric boundary conditions were applied on the symmetric surfaces, as shown in **Fig. S3 b**. Pollen and spore exine shells with representative shapes and sizes were directly extracted from the SEM images (Fig. 3). In order to measure the thickness of both exine and intine layers, the freeze-dried pollen and spore samples were fractured. Then, multiple locations of the fractured cross-sections were observed for measurements. Twenty grains were used for statistical analyses. *Camellia* pollen grains and *Lycopodium* spores have the same average radius, $R_{Cam} = R_{Lyo} = 16\ \mu m$. The average thickness of *Lycopodium* exine was found to be $T_{Lyo} = 64\ \mu m$, whereas that of *Camellia* was $T_{Cam} = 73\ \mu m$. The conical tip-angle θ of the *Lycopodium* trilete scar was assumed to be 30°, based on the image analysis. To avoid severe stress concentration during aperture opening in the *Camellia* pollen grain, we introduced tiny holes with radii of $R_{round} = 0.5\ \mu m$ around the aperture tips. Additionally, to avoid convergence problems, a finer mesh size was used around the tip regions of the apertures. A general mesh size of 0.1 μm was set, and thus the total number of elements for the *Camellia* and *Lycopodium* models were 27,276 and 34,492, respectively. We also implemented the widely used smooth step technique [52] to the load application, such that the inflating pressure was non-linearly loaded.

As *Camellia* and *Lycopodium* shells are not spherical, we only measured the maximum projected expansion radius (R_{swell}) in a two-dimensional plane from the optical images, as shown in **Fig. S3 a.** Both the *Camellia* pollen and *Lycopodium* spores experienced non-uniform expansion, due to the mechanical reduction of their apertures and irregular shapes. Thus, to fairly compare the computed three-dimensional shapes of the two pollen species to our experimental observations, we first defined the polar expansion radius (R_p) and equatorial expansion radius (R_e), as shown in **Fig. S4.** For simplicity, we also denoted the nondimensional expansion ratios at the polar view (λ_p) and the equator view (λ_e), which we obtained from R_p and R_e divided by the original radius of *Camellia* and *Lycopodium* grains, with $R_{Cam} = R_{Lyo} = 16\ \mu m$. We followed the same methodology as in our previous publication [15] for examining the large deformation of *Camellia* pollen, and thus used an explicit FEM method, although we induced the kinetic effect To achieve a quasi-static solution, a pseudo step time was set to 30 μs in simulation, which was slow enough to minimize kinetic energy and small enough to conserve computing resources.[15,52] The kinetic energy density observed in the deformed pollen and spore models was negligible, allowing us to exclude the kinetic effect from our measurement of the overall strain energy density due to deformation (**Fig. S5 a**). Hence, most of the external work done on the pollen and spore models was transferred into the recyclable internal energy of the pollen grains, leading to inflation/deflation of the pollen and spore exine models. The artificial energy associated with highly distorted meshes was less than 5% of the total strain energy, and thus was negligible (**Fig. S5 b)** [15,52]. The *Camellia* pollen exhibited a maximum expansion ratio of up to 1.43, whereas that of the *Lycopodium* spore only reached up to approximately 1.06, and was omittable, as shown in **Fig. S5 c**. The maximum inflation pressure of 8.3 MPa (at pH 14) led to maximum expansion of the *Camellia* pollen and *Lycopodium* spore models, showing good agreement with the experimental results.

2.7.5. Aperture opening FEA model for lycopodium spores

To mimic the germination process of intact *Lycopodium* spores, we developed a new exine FEA model in which we varied two key parameters, the continuity and stiffness of the connective tissue at the aperture region. The previous *Lycopodium* spore exine model was assumed to have perfectly bonded apertures, based on the experimental observation. However, in nature, the aperture opening of a *Lycopodium* spore is a key process of germination. Thus, through parametric study, we introduced the suture at the aperture regions, such that it gradually became softened and discrete in the current spore model, which uses a cohesive model with a traction-separation law for the aperture sutures [53,54]. The Young's modulus and length of the aperture suture were denoted as E_a and L_a, and the length of the periodic discrete region caused by the sutures was L_d. The Young's modulus of the spore wall was E_w, the same as that of the exine. The stiffness ($A_m = k_a/k_w$) and suture ($A_s = L_a/L_d$) ratios between the aperture and spore wall were also defined, to explore how the stiffness and continuity of aperture sutures affected the aperture-opening mechanism. The stiffnesses of the aperture suture, k_a, was defined as the Young's modulus of an aperture suture, E_a, divided by the constant thickness of 10^{-3} μm, which equals 1% of the characteristic element size (0.1 μm). Thus, the existence of the sutures at the aperture region did not affect the expansion of the *Lycopodium*

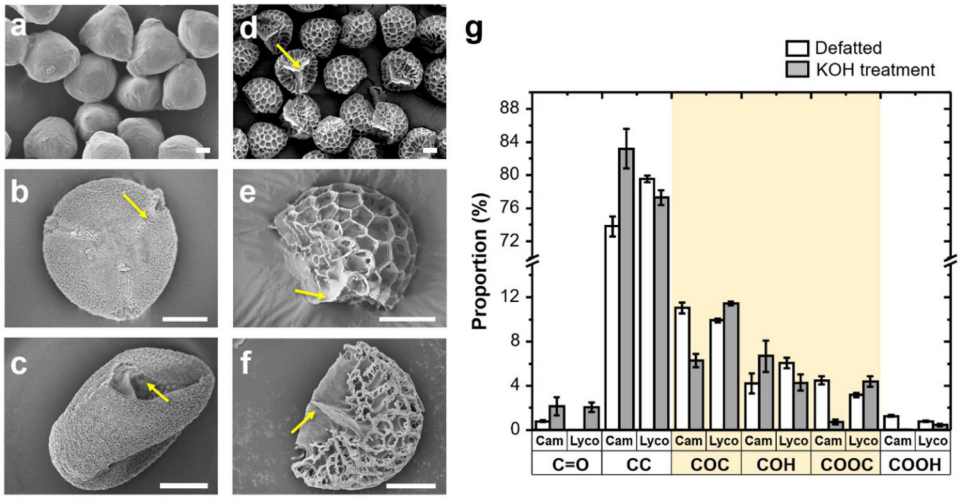

Fig. 3. Pollen and spores, before and after various chemical treatments. **a,** Natural *Camellia* pollen. **b,** Defatted *Camellia* pollen with acetone. **c,** KOH-treated *Camellia* pollen (24 h). **d,** Natural *Lycopodium* spore. **e,** Defatted *Lycopodium* spore with acetone. **f,** KOH-treated *Lycopodium* spore (24 h). (Scale bars, 10 μm). **g,** X-ray photoelectron spectroscopy-based analysis of oxygen- and carbon-containing functional groups of defatted and base-hydrolyzed pollen grains from various plant species. The proportions of different types of bonds before and after alkaline (KOH) hydrolysis are normalized.

spores due to their volume fraction. As a result, when $A_m = 1$ and $A_s = \infty$, this model was consistent with the previous exine FEA model that had perfectly bonded apertures. The cohesive thickness was carefully chosen, to ensure that the stiffness was high enough to prevent the artificial disturbance of apertures during the expansion of the *Lycopodium* spore [55]. The tri-aperture sutures on the *Lycopodium* spore became thinner, fractured, and degraded during immersion in several physiological solutions or during natural germination, leading to aperture opening. Some softening methods of aperture stiffness have been investigated, to determine the unfolding mechanisms of pollen grains [34,35,56]. In this study, we chose three representative aperture modulus ratios (A_m) with respect to the modulus of *Lycopodium* spores, as listed in **Table S2.** In addition to the stiffness ratio of the spore wall to the aperture suture, we also investigated the continuity of aperture sutures. $A_s = \infty$ represented a fully continuous and bonded aperture. Four typical values of A_s are listed in **Table S2**. $A_s < 1.0$ indicates the presence of discontinuous apertures, whereas $A_s > 1.0$ indicates the presence of relatively well-connected and bonded apertures. **Fig. S6** displays the maximum opened apertures of a *Lycopodium* spore with softened aperture stiffness, which was defined as the opened aperture ratio (A_o), obtained from the separation length between apertures (δ) divided by the radius of the spore (R_{Lyc}). Two expansion ratios, λ_p and λ_e, were also used to describe the expasion of spore models with opened apertures.

Stress induced by proton- and/or metallic-cation complexation [45] has been observed in plant tissues, such as cell walls, pollens, pollen tubes, stalks, and woody stems, in response to biotic stimuli (e.g., salt, drought, wounds, temperature changes, and growth) and abiotic chemical treatments (e.g., pH change and Ca^{2+}/EDTA treatment) [15,46,47]. As shown in the two-dimensional schematics of a pollen grain in **Fig. S2**, typical pollen and spore shells are composed of an intine and an exine. The sporopollenin-based exine is the first line of defense, as it blocks the flow of ions or water and provides mechanical support to the shell. In contrast, after absorbing water and under ion interaction, the intine, which contains the cellulose fiber-reinforced pectin, produces and transmits a force that pushes into the exine [12]. **Fig. S2** shows a pollen grain in a stressed state due to biotic or abiotic-induced deformation. The swellable intine efficiently transfers the coupled turgor and osmosis pressures to the exine, initiating the aperture opening of the pollen and spore grains. This process subjects the exine to the radical stress σ_r and loop stress σ_θ, as it undergoes radical expansion due to increased internal pressure, which is accelerated by excessive water uptake (**Fig. S5 b**). Nevertheless, the layer thickness of the exine, $r_k - r_j$, and the layer thickness of the intine, $r_j - r_i$, are extremely small compared to the radius of the entire pollen shell, where r_i, r_j is the radius of the inner and outer intine surfaces. For instance, a *Camellia* pollen grain has an intine thickness of ~0.08 μm and an exine thickness of ~0.73 μm, and a shell radius of ~16 μm. Hence, the radial stress σ_r is insignificant and thus negligible for these shell-walled structures [48,49]. **Fig. S5 c-d** compares the natural pollen and spore systems during germination with artificially transformed pollen microgels during swelling [9,15]. Both illustrations show similar boundary conditions, although the factors that triggered the shell expansion were different. The key membrane tensile stress, shown as σ_θ in the schematic illustration, was induced by opening the nanoscale water/ion channels and apertures, facilitating the expansion of the living pollens during germination [5,34] and the changes in the bioinspired pollen microgels under pH or ionic treatments [15,40]. To simulate the swelling/deswelling of pollen grains and pollen microgels, we developed finite element analysis (FEA) models of the exine with the boundary conditions calculated or derived from the multiphysics models of the intine under different pH conditions. **Fig. S5 e** illustrates the exine structure in the FEA simulations of the swelling/de-swelling of *Camellia* pollen and *Lycopodium* spores. The tri-aperture on the exine was modeled with the contact cohesive interaction set for weakly or strongly bonded interfaces, which varied according to the deformation of the shells of *Camellia* pollen and *Lycopodium* spores. The expansion boundary conditions of the exine from *Camelia* pollen and *Lycopodium* spores were based on the magnitude of σ_θ or swelling pressure, $P_{i,\,swelling}$, which was determined from the multiphysics models of the intine. Details of the overall approach behind the multiphysics model for intine layer and finite element analysis (FEA) for exine layer are described in Supplementary Methods.

2.8. Statistical analyses

Statistical analyses were performed using the Origin 2018 software package (OriginLab). An unpaired Student's *t*-test and one-way analyses of variance with Tukey's multiple comparison tests were used to calculate statistical significance; a *p* value of less than

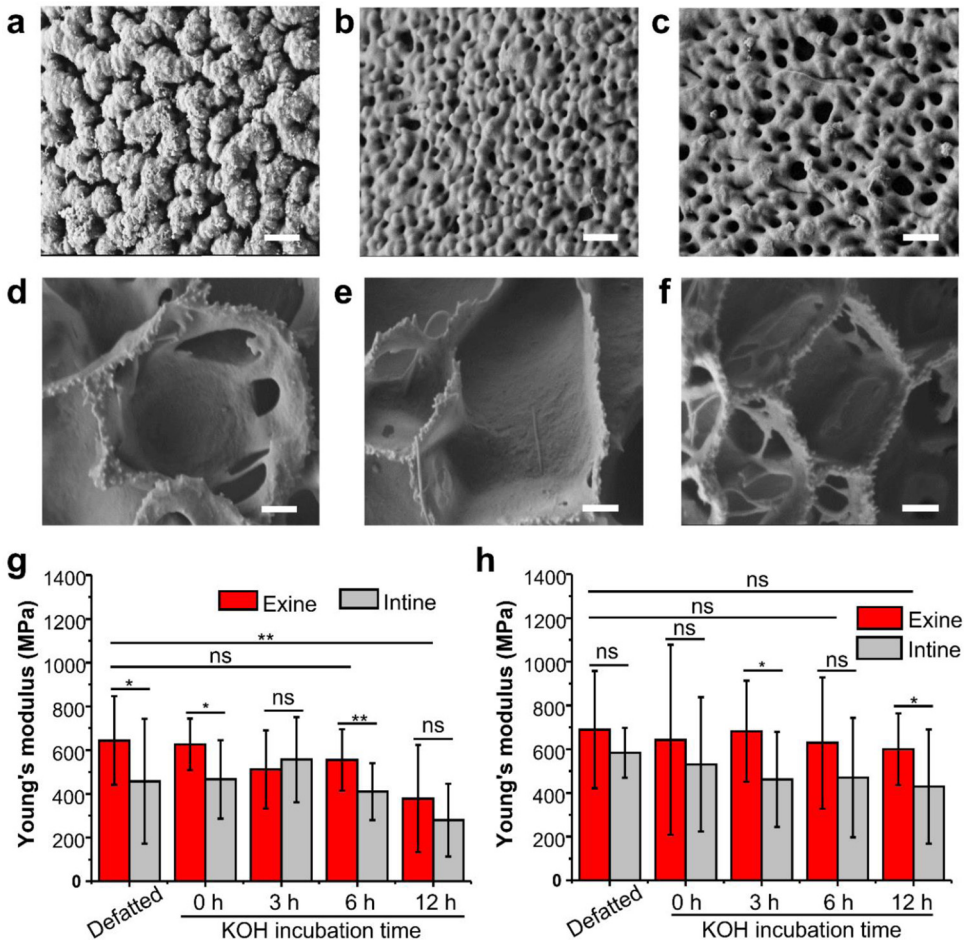

Fig. 4. Evolution of surface morphology and mechanical performance of KOH-treated pollen and spores over different incubation times. **a,** Surface morphology of defatted *Camellia* pollen. **b,** Surface morphology of 3-h KOH-treated *Camellia* pollen. **c,** Surface morphology of 12-h KOH-treated *Camellia* pollen. **d,** Surface morphology of defatted *Lycopodium* spore. **e,** Surface morphology of 3-h KOH-treated *Lycopodium* spore. **f,** Surface morphology of 12-h KOH-treated *Lycopodium spore*. (Scale bars = 1 μm) **g,** Atomic force microscopy (AFM)-characterized modulus of wet *Camellia* pollen. **h**, AFM-characterized modulus of wet *Lycopodium* spores. $^{*}p < 0.05$, $^{**}p < 0.01$, ns: not significant.

0.05 was considered statistically significant. The data are presented as the mean ± standard deviation, wherever appropriate.

3. Results and discussion

3.1. Structural changes in pollen grains after microgel formation

First, we observed morphological changes of the exine layer and apertures in *Camellia* pollen and *Lycopodium* spores, as model systems, before and after chemical treatments. *Camellia* pollen is tricolporate and spherical, with an average diameter of ~ 32 μm, as shown in Fig. 3a. Its surface is smooth, with a perforated tectum. Fig. 3b shows the three closed apertures and perforated tectum of a spherical *Camellia* pollen grain after it has been defatted with acetone. However, the alkaline treatment damaged the *Camellia* pollen shell, opening its apertures and weakening the shell structure. Thus, the dehydrated pollen shell collapsed, losing its spherical shape (as shown in Fig. 3c **and Fig. S7**). In marked contrast, *Lycopodium* spores exhibited no significant morphological changes after both defatting and alkali treatments, retaining their reticulated architecture and inflated trilete scar (**Figs. 3d-f and Fig. S7**) [47,57,58].

As the structural integrity of a pollen shell originates from the strong polymer network and mechanical stability of the sporopollenin in the exine, we speculated that alkaline treatment caused significant changes occurred in the sporopollenin structures in the exine of *Camellia* pollen, but not in that of *Lycopodium* spores. X-ray photoelectron spectroscopy (XPS) was used to analyze the surface of *Camellia* pollen and *Lycopodium* spores, to determine the bonding states of carbon (C) and oxygen (O) in the exine layer. As shown in the XPS-based analysis in Fig. 3g, sporopollenin exine has a complicated chemical structure, mainly composed of a backbone of straight, branched, or cyclic aliphatic chains linked with saturated or unsaturated fatty acids via ester bonds (COOC) [4,59,60]. Those aliphatic backbones are also highly cross-linked via ether bonds (COC), which provides additional mechanical and chemical stability [4,60]. Thus, the loss or reduction of ester and ether bonds can indicate sporopollenin degradation [4,59,60]. A significant reduction in ester and ether bonds was observed in alkaline-treated *Camellia* pollen, resulting in an increase in the number of hydroxyl groups (OH) and a decrease in the number of carboxyl groups (COOH). The alkaline hydrolysis of ester bonds released free fatty acids from the sporopollenin, restoring the hydroxyl groups of the aliphatic backbones. The reduction of ether bonds may also lead to reduced cross-linking densities in the aliphatic backbone.

In contrast, *Lycopodium* spores show almost no pronounced changes in either ester or ether bond patterns after alkaline treatment but did show changes in their carbonyl groups (C = O). It has been well-established that carboxylates form in KOH-treated *Lycopodium* spores, which increases the hydrophilicity of the spore surface [58]. We found similar trends in other pollen and spore

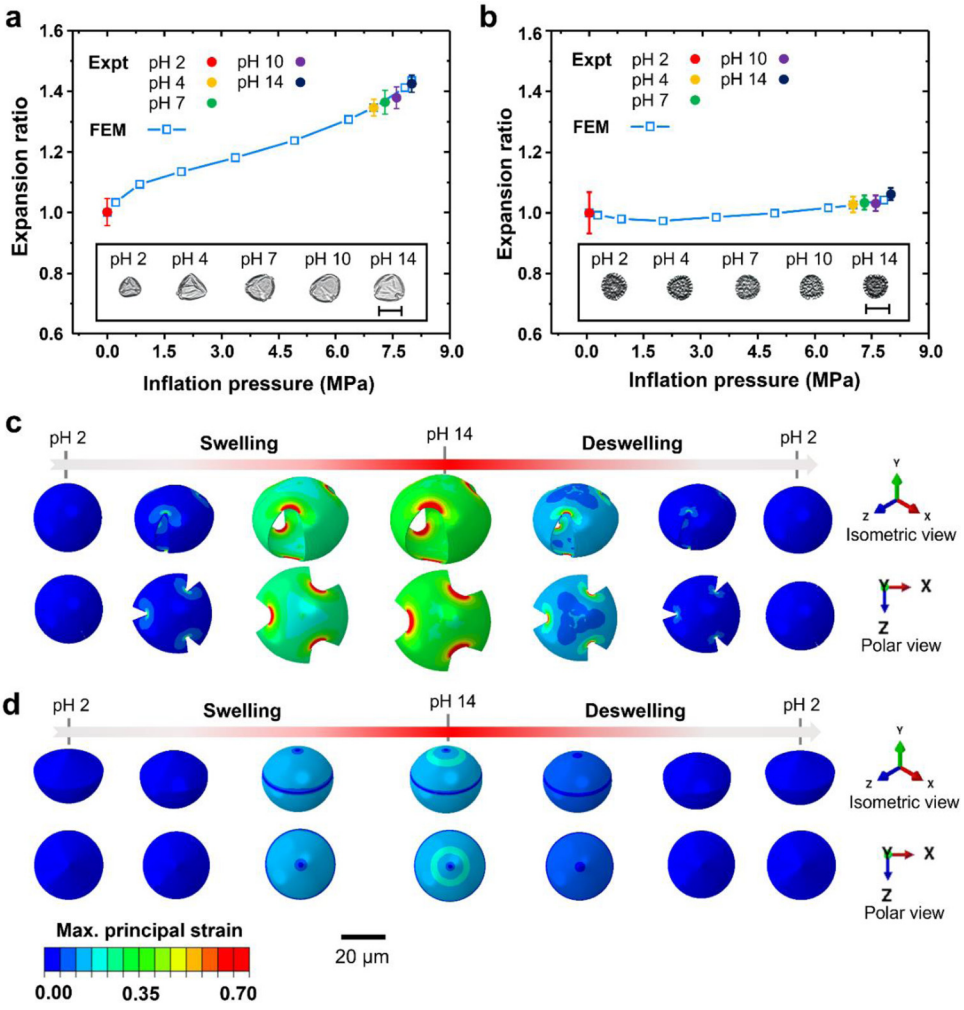

Fig. 5. Comparison of pH response in the experimental and finite element method (FEM)-simulated results for chemically treated soft *Camellia* pollen grains and *Lycopodium* spores. **a,** Expansion ratios of 6-h KOH-treated *Camellia* pollen microgels, in terms of swelling pressure induced by pH change. **b,** Expansion ratios of 6-h KOH-treated *Lycopodium* spore, in terms of swelling pressure induced by pH change. **c,** Strain contours of 6-h KOH-treated *Camellia* pollen microgel, from pH 2 to pH 14. **d,** Strain contours of 6-h KOH-treated *Lycopodium* spore from pH 2 to pH 14. The large local deformation was concentrated at the trilete scar region.

species (**Fig. S8**). The post-alkaline-treatment chemical structures of pollens of two other species (*Baccharis* and *Helianthus*) from the eudicot clade, and non-gelated pollens and spores from *Typha* (monocot) and *Pinus* (gymnosperms), were compared with that of *Lycopodium* spores. In the eudicot pollen grains, there was a significant reduction in the number of ether and ester bonds, and an increase in the number of hydroxyl groups, whereas in the monocot pollens and the gymnosperms spores there was only a pronounced increase in the number of ester bonds.

3.2. Mechanical performance of transformed pollen and spores

Changes in the chemical structures of the sporopollenin of the different pollen and spore systems led to different surface morphological and mechanical alterations, as shown in Fig. 4. As expected, the alkaline hydrolysis of ester and ether bonds led to a significant loss of fatty acids, and thus a reduction in the cross-linking density of sporopollenin backbones in *Camellia* pollen. As a result, the perforated tectum of *Camellia* pollen exine became thinner and more porous, losing significant matrix components (Fig. 4a-c; **Fig. S9**). In contrast, although the honeycomb-like ridges atop *Lycopodium* pollen exine became more porous with prolonged KOH treatment, the exine shell remained almost intact and showed no significant morphological changes (Fig. 4d-f), which was consistent with the details visible in Fig. 4f. We used atomic force microscopy (AFM) to measure the Young's moduli of the exine and intine of *Camelia* pollen and *Lycopodium* spores as a function of alkaline-treatment time. The degraded sporopollenin of *Camellia* exine showed significantly decreased Young's moduli after prolonged alkaline treatment, from ~650 MPa for the exine of defatted pollen to ~400 MPa for the exine of 12-h KOH-treated pollen (Fig. 4g **and Fig. S10**). However, the average Young's moduli of KOH-treated *Lycopodium* exine (650–700 MPa) were similar to those of defatted *Lycopodium* exine, regardless of the KOH treatment time (Fig. 4h). Moreover, in case of *Camellia* pollen, the ratio of the average Young's moduli of the exine to that of the intine ($M_{E/I}$) tended to decrease with KOH treatment, from ~1.7 (defatted pollen) to ~ 1 (12 h KOH-treated pollen) even through this mechanical change wasn't as drastic as that of sunflower pollen [15]. The defatted exine of sunflower pollen was much stiffer than that of *Camellia* pollen, thus sunflower exine must be subjected to greater softening than *Camellia* exine.

3.3. Morphological basis of the difference between pollen and spore volume expansion in an acidic environment

Angiosperms dominate the Earth's surface: most green plants in all environments are angiosperms, and they exist in more ex-

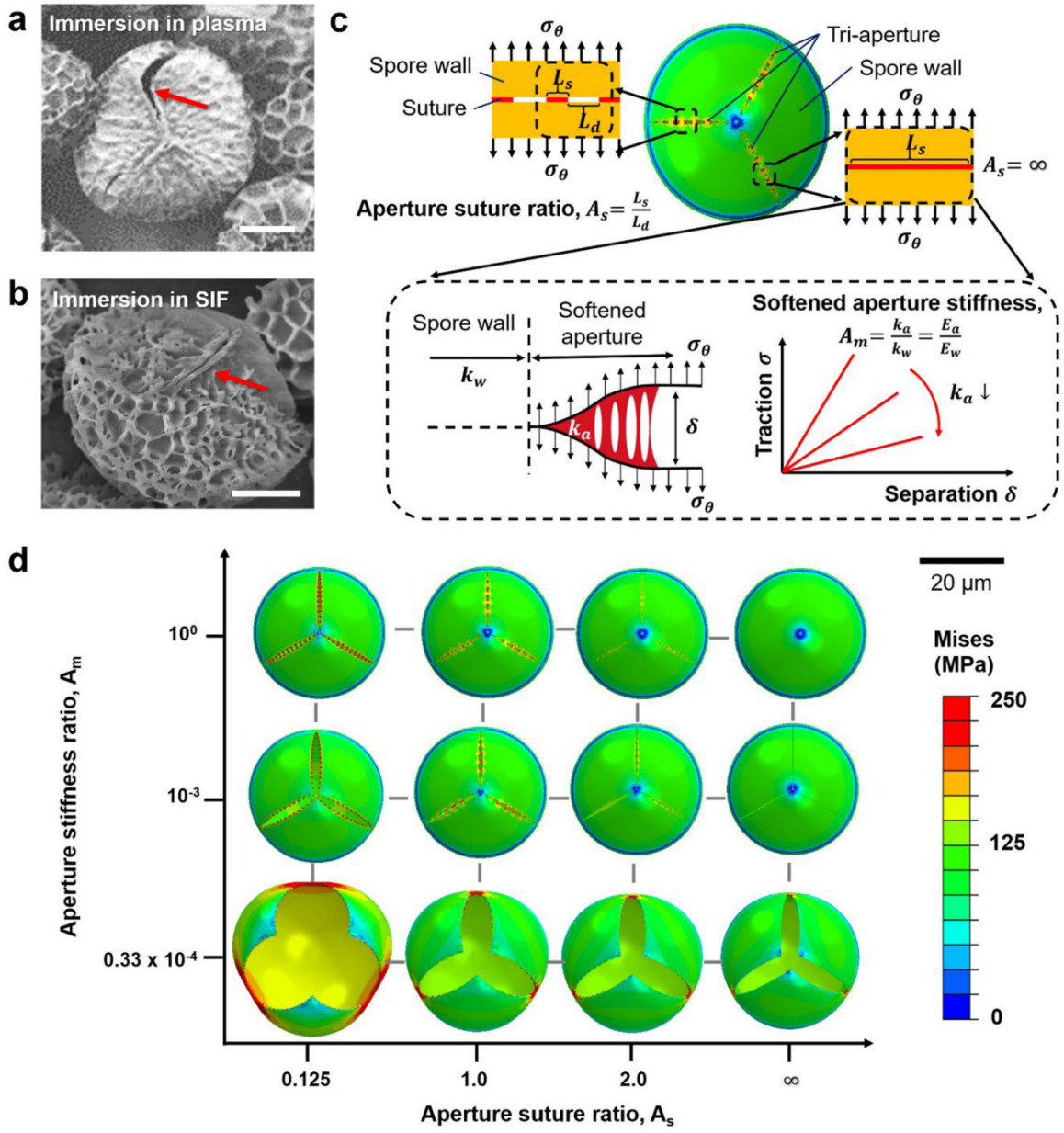

Fig. 6. Softened aperture stiffness-driven volume expansion and morphology of *Lycopodium* spores. **a-b,** Scanning electron microscopy images of *Lycopodium* spores with weakened, slightly opened apertures after immersion in different body fluids. **c,** Cohesive sutured aperture model for *Lycopodium* spores, with the traction-separation law applied at the aperture suture. The model involves the traction σ_θ (loop stress) and separation δ (distance between two interfaces of an aperture), where apertural stiffness, k_a, is defined as the aperture modulus (E_a) divided by a constant cohesive thickness. In addition, sutures with length, L_s, alternating with discontinuous parts (length L_c) are found on the *Lycopodium* apertures. The aperture suture ratio, A_s, is defined as L_s/L_d, and a perfectly bonded aperture has an $A_s = \infty$. **d,** Morphology diagram and von Mises stress contours of the volume expansion and aperture opening of a *Lycopodium* spore with a softened aperture stiffness in the (A_s, A_m) plane, shown in a polar view. SIF = simulated intestinal fluid; L_s = length of an aperture suture; L_d = length of a periodic discontinuous region; E_a =Young's modulus of an aperture suture; E_w = Young's modulus of a spore wall; k_a = stiffness of an aperture suture; k_w = stiffness of a spore wall.

treme environments than any other group of plants [61]. *Camellia* are angiosperms and *Lycopodium* are gymnosperms and produce sexual reproduction units (pollen) and asexual reproduction units (spores), respectively. Like sunflower pollen, *Camellia* pollen has symmetrical tri-apertural geometry and undergoes significant structural and mechanical alterations during alkaline treatment. In contrast, *Lycopodium* spores are asymmetric, with an inflated trilete scar on their proximal face and pronounced reticulated architecture on their distal face, and the mechanical behavior of their exine is unchanged by alkaline treatment. These structural and mechanical differences influence the responses of these two species to environmental stimuli.

To understand the underlying stimulus-responsive swelling and deswelling mechanisms of *Camellia* pollen and *Lycopodium* spores, we developed FEA models in conjunction with a multiphysics model (**Figs. S2-3**).[15] The multiphysics model of de-esterified intine was used to predict the internal hydrostatic tensile force due to osmotic pressure, based on pH-dependent ionic concentrations of aqueous solutions. Fig. 5 compares the simulated results and experimental measurements for *Camellia* pollen and *Lycopodium* spores after 6 h of KOH treatment. Two distinguishable dimensionless expansion or swelling ratios of the pollen and spores were studied: the equatorial swelling ratio (λ_e) and the polar swelling ratio (λ_p), due to asymmetric 3D structures of pollen and spores,

where λ_e and λ_p are defined as R_e/R and R_p/R, and R_e, R_p and R denote the expanded radii of the polar and equatorial planes, and the average pollen or spore radius, respectively (**Fig. S6**). However, our experimental observations were based on the swelling ratios at the maximum projection of the pollen and spore contours; thus, the experimental swelling ratios (λ) were closer to the λ_e values of the FEA models in Fig. 5a and **b**, which were larger than the λ_p values. The simulation results for *Camellia* and *Lycopodium* were in a good agreement with their corresponding experimental results. *Camellia* pollen exhibited a maximum equatorial swelling ratio ($\lambda_{e,\,max}$) of ~1.4, whereas *Lycopodium* spores did not swell, resulting in a constant swelling ratio (λ) of ~1.0 regardless of pH changes.

The strain and stress contours of the two systems gave clues about the deformation mechanisms that drove the swelling-deswelling process in response to pH changes, as shown in Figs. 5c and **d,** and **Fig. S11**. *Camellia* pollen accommodated its large deformation in its three apertures, and due to its oblate shape, λ_e and λ_p varied with the expansion of the pollen shell. In contrast, the asymmetry of *Lycopodium* spores resulted in deformation concentrating around their proximal face, at the location of the inflated trilete scar. Thus, even though the projected spore diameters remained the same during swelling, they were nevertheless deformed (Fig. 5d). As a result, *Lycopodium* spore shells retained a near-ideal spherical shape, with the value of λ_p approximately equal to the value of λ_e. The deformation of spore shells was also highly localized around apertures, and thus the accumulated strain energy in these regions affected the germination of *Lycopodium* spores. We believe that these different deformation mechanisms are closely correlated with the reversible and irreversible germination processes, because of the structure–property–performance relationship of these natural systems. This provides insight into the survivability traits of diverse plant species [62]. We also examined this highly localized deformation of *Lycopodium* spores in conjunction with their germination scheme, by simulating the rupture and opening of the trilete scar.

3.4. Tricolpate opening induced by apertural softening in Lycopodium *spores*

In contrast to *Camellia* pollen, *Lycopodium* spores have a solid and rigid exine that is resistant to alkaline hydrolysis; in particular, the trilete apertures remain closed when spores are treated with alkaline solutions [15,57,58]. However, immersion in body fluids, such as blood plasma or simulated intestinal fluid (SIF), typically ruptures the aperture region, causing spores to open (Fig. 6a, b). Crucially, the rupture or breakage of these apertures is required for a spore to germinate and grow into a gametophyte called a prothallus, which is the natural mode of fertilization of non-seed vascular plants [24]. In the early stage of spore germination, the opening of apertures is essentially a biophysical or biomechanical process [63] that involves divided cells that have outgrown the capsule being pushed from the spore [62]. The outermost spore cortex is degraded and softened by hydrolysis, and subsequently absorbs a nutrient germinant that is associated with the release of ionic components. The spore then begins to absorb more water, inducing significant osmotic pressure and subsequently initiating spore germination [63,64]. Accordingly, we modeled the fracture mechanism of a spore by modulating the stiffness and structure of the connective tissue between aperture plates, as illustrated in Fig. 6c. During SIF treatment, the spore apertures were prone to partial rupture, as shown in Fig. 6b. Thus, we considered two parameters for the relationship between the aperture and spore wall: the aperture suture–connectivity (aperture suture ratio, A_s) and the stiffness ratio (aperture modulus ratio, i.e., A_m = Young's modulus of the aperture suture/Young's modulus of the spore wall). In response to hypothetical turgor/swelling pressure from the intine, the connectivity and stiffness of the connective tissue varied from fully connected (∞) to partially connected ($A_s = 0.125$), and from rigid ($A_m = 1$) to very soft ($A_m = 1/3 \times 10^{-4}$). The induced local deformation around the aperture region, which is visible in Fig. 5, generated fractures at the apertures as A_m and A_s decreased in magnitude. The suture regions of the rigid seed coat plates were thus disconnected and weakened during seed germination [65]. Consequently, we speculate that the sutures of spore apertures undergo changes similar to those of seed coat sutures.

Clearly, the connectivity and stiffness ratios of the aperture-connective tissue systems both played significant roles in the mechanism of *Lycopodium* spore fracture during germination, as shown in Fig. 6d and **Fig. S12**. In the case with $A_s = \infty$ and $A_m = 1$, the apertures of *Lycopodium* spores remained intact prior to any sign of germination: no fracture was observed. A_s is a measure of the irregularity of spore apertures, and A_m is a measure of the hydrolysis-induced softening of spores upon exposure to agents such as enzymes or nutrient germinants. Thus, the results showed that the degradation of connective tissue is due to increases in its discontinuity and decreases in its strength, which indicates that spores experience more significant aperture opening than pollen. For many biological materials, the stiffness ratio between the hard phase and soft phase is known to be between $\sim10^{-2}$ - $\sim10^{-3}$ [66]. Through the degradation, this ratio may be significantly reduced [67]. The interaction of weakening and local breakage of these apertures in the proximal region of spores is an efficient strategy for spore germination [24,27,67,68]. Thus, the rupturing of spores may be facilitated via aperture opening and closing due to the expansion and contraction of de-esterified intine [15], without significant changes in spore volume, in contrast to the swelling-driven expansion of pollen.

Conclusion

In this study, we studied *Camellia* pollen grains and *Lycopodium* spores as representative models of grains that form and do not form microgel particles, respectively, to characterize the fundamental structure–property relationships associated with germination-related shape transformations, and the chemical processes underlying these processes. Upon alkaline incubation, symmetrical *Camellia* pollen grains were transformed into microgel particles, due to weakening of their exine, and de-esterification and subsequent swelling of their intine. However, upon alkaline incubation, *Lycopodium* spores did not undergo extensive structural changes. Computational modeling provided insights into the mechanisms and pH-dependence of changes in the shape and material properties of the specimens and agreed well with the experimental observations. Notably, the model predicted that there was local deformation of *Lycopodium* spore shells in their proximal region, due to their asymmetric shell structures. The spores also exhibited significant fracture of their apertures when immersed in SIFs, and such breakage events were necessary to facilitate irreversible germination processes. These modeling efforts also revealed how varying the connectivity and rigidity of the material interface between three closed apertures could trigger spore opening via a combination of highly localized deformation and osmotic pressure gradients in the intine. Collectively, these findings offer insights into how pollen grains and spores could be transformed into biomimetic materials with apertures that open and close in response to environmental stimuli. Such germination-type processes could therefore be harnessed to develop new classes of intelligent sensors and actuators.

Data availability

The raw data required to reproduce this study is available from S.J and C.N.-J. on reasonable request.

Declaration of Competing Interest

Authors have no conflict of interest to disclose.

Acknowledgments

This research was supported by Advanced Manufacturing and Engineering Individual Research Grants (AME IRG) (A1983c0031) through the Agency for Science, Technology and Research (A*STAR).

Supplementary materials

Supplementary material associated with this article can be found, in the online version, at doi:10.1016/j.apmt.2022.101471.

References

[1] H.J.B. Birks, H.H. Birks, B. Ammann, The fourth dimension of vegetation, Science 354 (2016) 412–413.
[2] T. Ariizumi, K. Toriyama, Genetic regulation of sporopollenin synthesis and pollen exine development, Annu. Rev. Plant Biol. 62 (2011) 437–460.
[3] P. Guzman-Delgado, M.A. Zwieniecki, The makeup of a gamete space capsule, Nat. Plants 5 (1) (2019) 8.
[4] F.S. Li, P. Phyo, J. Jacobowitz, M. Hong, J.K. Weng, The molecular structure of plant sporopollenin, Nat. Plants 5 (1) (2019) 41–46.
[5] J.K. Muhlemann, T.L.B. Younts, G.K. Muday, Flavonols control pollen tube growth and integrity by regulating ROS homeostasis during high-temperature stress, Proc. Natl. Acad. Sci. USA 115 (47) (2018) E11188–E11197.
[6] O.A. Volkova, E.E. Severova, S.V. Polevova, Structural basis of harmomegathy: evidence from *Boraginaceae* pollen, Plant Syst. Evol. 299 (9) (2013) 1769–1779.
[7] J. Heslop-Harrison, Y. Heslop-Harrison, Germination of stress-tolerant eucalyptus pollen, J. Cell Sci. 73 (1) (1985) 135–157.
[8] A. Geitmann, J.K. Ortega, Mechanics and modeling of plant cell growth, Trends Plant Sci 14 (9) (2009) 467–478.
[9] D.J. Cosgrove, Plant cell wall extensibility: connecting plant cell growth with cell wall structure, mechanics, and the action of wall-modifying enzymes, J. Exp. Bot. 67 (2) (2016) 463–476.
[10] L.P. Taylor, P.K. Hepler, Pollen germination and tube growth, Annu. Rev. Plant Physiol. Plant Molec. Bio. 48 (1) (1997) 461–491.
[11] E.S. Weinberg, B.R. Voeller, Induction of fern spore germination, Proc. Natl. Acad. Sci. USA 64 (3) (1969) 835–842.
[12] E.S. Hamilton, G.S. Jensen, G. Maksaev, A. Katims, A.M. Sherp, E.S. Haswell, Mechanosensitive channel MSL8 regulates osmotic forces during pollen hydration and germination, Science 350 (6259) (2015) 438–441.
[13] M.A. Zwieniecki, P.J. Melcher, N.Michele Holbrook, Hydrogel control of xylem hydraulic resistance in plants, Science 291 (5506) (2001) 1059–1062.
[14] K.T. Haas, R. Wightman, E.M. Meyerowitz, A. Peaucelle, Pectin homogalacturonan nanofilament expansion drives morphogenesis in plant epidermal cells, Science 367 (6481) (2020) 1003–1007.
[15] T.F. Fan, S. Park, Q. Shi, X. Zhang, Q. Liu, Y. Song, H. Chin, M.S.B. Ibrahim, N. Mokrzecka, Y. Yang, H. Li, J. Song, S. Suresh, N.J. Cho, Transformation of hard pollen into soft matter, Nat. Commun. 11 (1) (2020) 1449.
[16] A.F. Edlund, R. Swanson, D. Preuss, Pollen and stigma structure and function: the role of diversity in pollination, Plant Cell 16 (Suppl_1) (2004) S84–S97.
[17] J. Heslop-Harrison, Supplement 1: aspects of the structure, cytochemistry and germination of the pollen of rye, Ann. Bot. 44 (1979) 2–47.
[18] J. Heslop-Harrison, Pollen germination and pollen-tube growth, in: G.H. Bourne, K.W. Jeon, M. Friedlander (Eds.), Int. Rev. Cytol., Academic Press, 1987, pp. 1–78.
[19] A. Peaucelle, S. Braybrook, H. Hofte, Cell wall mechanics and growth control in plants: the role of pectins revisited, Front. Plant Sci. 3 (2012) 121.
[20] G.M. Zinkl, B.I. Zwiebel, D.G. Grier, D. Preuss, Pollen-stigma adhesion in Arabidopsis: a species-specific interaction mediated by lipophilic molecules in the pollen exine, Development 126 (23) (1999) 5431–5440.
[21] M. Golovkin, A.S.N. Reddy, A calmodulin-binding protein from *Arabidopsis* has an essential role in pollen germination, Proc. Natl. Acad. Sci. USA 100 (18) (2003) 10558–10563.
[22] R.C. Mundargi, Extraction of sporopollenin exine capsules from sunflower pollen grains, RSC Adv 6 (2016) 16533–16539.
[23] G. Mackenzie, A.N. Boa, A. Diego-Taboada, S.L. Atkin, T. Sathyapalan, Sporopollenin, the least known yet toughest natural biopolymer, Front. Mater. 2 (2015) 66.
[24] V. Raghavan, Cytology, physiology, and biochemistry of germination of fern spores, in: G.H. Bourne, J.F. Danielli, K.W. Jeon (Eds.), Int. Rev. Cytol., Academic Press, 1980, pp. 69–118.
[25] R.J. Scott, M. Spielman, H.G. Dickinson, Stamen structure and function, Plant Cell 16 (suppl 1) (2004) S46–S60.
[26] S. Blackmore, A.H. Wortley, J.J. Skvarla, J.R. Rowley, Pollen wall development in flowering plants, New Phytol 174 (3) (2007) 483–498.
[27] J.M. Tylianakis, The global plight of pollinators, Science 339 (6127) (2013) 1532–1533.
[28] S.A. Johnson, S. McCormick, Pollen germinates precociously in the anthers of raring-to-go, an *Arabidopsis* gametophytic mutant, Plant Physiol 126 (2) (2001) 685–695.
[29] E. Michard, A.A. Simon, B. Tavares, M.M. Wudick, J.A. Feijó, Signaling with ions: the keystone for apical cell growth and morphogenesis in pollen tubes, Plant Physiol 173 (1) (2017) 91–111.
[30] L.J.W. Gilissen, The influence of relative humidity on the swelling of pollen grains in vitro, Planta 137 (1977) 299–301.
[31] T. Higashiyama, H. Takeuchi, The mechanism and key molecules involved in pollen tube guidance, Annu Rev Plant Biol 66 (2015) 393–413.
[32] A.M. Chaudhury, A. Koltunow, T. Payne, M. Luo, M.R. Tucker, E.S. Dennis, W.J. Peacock, Control of early seed development, Annu. Rev. Cell Dev. Biol. 17 (1) (2001) 677–699.
[33] R. Finkelstein, W. Reeves, T. Ariizumi, C. Steber, Molecular aspects of seed dormancy, Annu Rev Plant Biol 59 (2008) 387–415.
[34] E. Katifori, S. Alben, E. Cerda, D.R. Nelson, J. Dumais, Foldable structures and the natural design of pollen grains, Proc. Natl. Acad. Sci. USA 107 (17) (2010) 7635–7639.
[35] A. Bozic, A. Siber, Mechanical design of apertures and the infolding of pollen grain, Proc. Natl. Acad. Sci. USA 117 (43) (2020) 26600–26607.
[36] A. Radja, E.M. Horsley, M.O. Lavrentovich, A.M. Sweeney, Pollen cell wall patterns form from modulated phases, Cell 176 (2019) 856–868 e10.
[37] J.A. Banks, Gametophyte development in ferns, Annu. Rev. Plant Physiol. Plant Molec. Bio. 50 (1) (1999) 163–186.
[38] Y. Xu, X. Cao, H. Zhao, E. Yang, Y. Wang, N. Cheng, W. Cao, Impact of camellia japonica bee pollen polyphenols on hyperuricemia and gut microbiota in potassium oxonate-induced mice, Nutrients 13 (8) (2021).
[39] R.C. Mundargi, M.G. Potroz, S. Park, J.H. Park, H. Shirahama, J.H. Lee, J. Seo, N.-J. Cho, Lycopodium spores: a naturally manufactured, superrobust biomaterial for drug delivery, Adv. Funct. Mater. 26 (4) (2016) 487–497.
[40] Z. Zhao, Y. Hwang, Y. Yang, T. Fan, J. Song, S. Suresh, N.J. Cho, Actuation and locomotion driven by moisture in paper made with natural pollen, Proc. Natl. Acad. Sci. USA 117 (16) (2020) 8711–8718.
[41] P.E. Jardine, F.A. Abernethy, B.H. Lomax, W.D. Gosling, W.T. Fraser, Shedding light on sporopollenin chemistry, with reference to UV reconstructions, Rev. Palaeobot. Palynol. 238 (2017) 1–6.
[42] J.F. Watts, J. Wolstenholme, An Introduction to Surface Analysis by XPS and AES, Wiley-VCH, 2003.
[43] Z. Zeng, J.-C. Tan, AFM nanoindentation to quantify mechanical properties of nano-and micron-sized crystals of a metal–organic framework material, ACS Appl. Mater. Interfaces 9 (45) (2017) 39839–39854.
[44] J.L. Hutter, J. Bechhoefer, Calibration of atomic-force microscope tips, Rev. Sci. Instrum. 64 (7) (1993) 1868–1873.
[45] G.T. Grant, E.R. Morris, D.A. Rees, P.J.C. Smith, D. Thom, Biological interactions between polysaccharides and divalent cations: the egg-box model, FEBS Lett 32 (1) (1973) 195–198.
[46] J.K. Zhu, Abiotic stress signaling and responses in plants, Cell 167 (2) (2016) 313–324.
[47] P. Gonzalez-Cruz, M.J. Uddin, S.U. Atwe, N. Abidi, H.S. Gill, A chemical treatment method for obtaining clean and intact pollen shells of different species, ACS Biomater. Sci. Eng. 4 (7) (2018) 2319–2329.
[48] G.A. Holzapfel, Hyperelastic Materials, Wiley, 2000.
[49] G.A. Holzapfel, T.C. Gasser, R.W. Ogden, A new constitutive framework for arterial wall mechanics and a comparative study of material models, J. Elast. 61 (1) (2000) 1–48.
[50] J. Bergström, Mechanics of Solid polymers: Theory and Computational Modeling, William Andrew, 2015.
[51] X. Liu, C. Steiger, S. Lin, G.A. Parada, J. Liu, H.F. Chan, H. Yuk, N.V. Phan, J. Collins, S. Tamang, Ingestible hydrogel device, Nat. Commun. 10 (2019).
[52] ABAQUSABAQUS 2017 User documentation, Dassault Systemes Simulia Corp., Providence, RI, 2017.
[53] K. Park, G.H. Paulino, Cohesive zone models: a critical review of traction-separation relationships across fracture surfaces, Appl. Mech. Rev. 64 (6) (2011) 060802.
[54] Y. Jia, H.-L. Wang, B. Liu, Y. Huang, H. Gao, Intrinsic-to-extrinsic transition in fracture toughness through structural design: a lesson from nature, Eng. Fract. Mech. 37 (2020) 100685.
[55] A. Turon, C.G. Dávila, P.P. Camanho, J. Costa, An engineering solution for mesh size effects in the simulation of delamination using cohesive zone models, Eng. Fract. Mech. 74 (10) (2007) 1665–1682.
[56] E. Couturier, J. Dumais, E. Cerda, E. Katifori, Folding of an opened spherical shell, Soft Matter 9 (34) (2013).
[57] R.C. Mundargi, M.G. Potroz, J.H. Park, J. Seo, E.L. Tan, J.H. Lee, N.J. Cho, Eco-friendly streamlined process for sporopollenin exine capsule extraction, Sci Rep 6 (2016) 19960.
[58] M.J. Uddin, N. Abidi, J. Warzywoda, H.S. Gill, Investigation of the fate of proteins and hydrophilicity/hydrophobicity of *Lycopodium clavatum* spores after organic solvent-base-acid treatment, ACS Appl. Mater. Interfaces 11 (23) (2019) 20628–20641.

[59] E. Domínguez, J.A. Mercado, M.A. Quesada, A. Heredia, Pollen sporopollenin: degradation and structural elucidation, Sex. Plant Reprod. 12 (3) (1999) 171–178.
[60] A. Mikhael, K. Jurcic, C. Schneider, D. Karr, G.L. Fisher, T.D. Fridgen, A. Diego-Taboada, P.E. Georghiou, G. Mackenzie, J. Banoub, Demystifying and unravelling the molecular structure of the biopolymer sporopollenin, Rapid Commun. Mass Spectrom. 34 (10) (2020) e8740.
[61] F. Berendse, M. Scheffer, The angiosperm radiation revisited, an ecological explanation for Darwin's 'abominable mystery, Ecol. Lett. 12 (9) (2009) 865–872.
[62] D. Bonazzi, J.D. Julien, M. Romao, R. Seddiki, M. Piel, A. Boudaoud, N. Minc, Symmetry breaking in spore germination relies on an interplay between polar cap stability and spore wall mechanics, Dev. Cell 28 (5) (2014) 534–546.
[63] A. Moir, How do spores germinate? J. Appl. Microbiol. 101 (3) (2006) 526–530.
[64] P. Setlow, Germination of spores of Bacillus species: what we know and do not know, J. Bacteriol. 196 (7) (2014) 1297–1305.
[65] B.P.J. Hasseldine, C. Gao, J.M. Collins, H.D. Jung, T.S. Jang, J. Song, Y. Li, Mechanical response of common millet (*Panicum miliaceum*) seeds under quasi-static compression: experiments and modeling, J. Mech. Behav. Biomed. Mater. 73 (2017) 102–113.
[66] U.G.K. Wegst, H. Bai, E. Saiz, A.P. Tomsia, R.O. Ritchie, Bioinspired structural materials, Nat. Mater. 14 (1) (2015) 23–36.
[67] M. Zarnkow, A. Mauch, W. Back, E.K. Arendt, S. Kreisz, Proso millet (Panicum miliaceum L.): an Evaluation of the Microstructural Changes in the Endosperm during the Malting Process by Using Scanning-Electron and Confocal Laser Microscopy, J. Inst. Brew. 113 (4) (2007) 355–364.
[68] P. Nick, Z. Opatrny, Applied Plant Cell Biology: Cellular Tools and Approaches for Plant Biotechnology, Springer Berlin Heidelberg, 2014.